Pergamon

Chaos, Solitons & Fractals Vol. 7, No. 7, pp. 991–1010, 1996

0960-0779/96 $15.00 + 0.00

0960-0779(95)00098-4

Magnetic Field Line Mappings for a Tokamak with Ergodic Limiters

I. L. CALDAS

Instituto de Física da Universidade de São Paulo C.P. 66318, 05389-970 São Paulo, Brazil

J. M. PEREIRA

Departamento de Física da Universidade Federal do Paraná C.P. 19081, 81531-990 Curitiba, Paraná, Brazil

K. ULLMANN

Instituto de Física da Universidade de São Paulo C.P. 66318, 05389-970 São Paulo, Brazil

and

R. L. VIANA

Departamento de Física da Universidade Federal do Paraná C.P. 19081, 81531-990 Curitiba, Paraná, Brazil

(Accepted 6 October 1996)

Abstract—An ergodic magnetic limiter is a device whose main effect in a tokamak is to create a cold boundary layer of chaotic magnetic field lines. In order to study its effect we have used two approaches. The first is a description of magnetic island formation through an analytical method to describe its dimensions, results being in accordance with numerical Poincaré maps for magnetic field lines. The second is a model which simulates the ergodic limiter action as a sequence of impulsive perturbations, enabling the derivation of analytical formulae for the Poincaré maps. Copyright © 1996 Elsevier Science Ltd.

INTRODUCTION

The problem of the quality of plasma confinement in a fusion-oriented device like a tokamak has many facets, challenging us with both conceptual and technical difficulties to be solved. Thus, the presence of impurities in the confined plasma should be controlled to improve the confinement [1, 2]. However, a common source of impurities in tokamak plasmas is the heat and particle loadings on the metallic inner wall, causing impurity release by sputtering processes. In the late seventies some authors [3, 4] proposed that a cold boundary layer of chaotic magnetic field lines could act as a plasma limiter, since it would uniformize these loadings, lowering the impurity levels within the plasma core.

The ergodic magnetic limiter concept [5] is based on the idea that a chaotic boundary layer of field lines could appear as a result of magnetic island interaction in the peripheral region of the tokamak chamber. But these islands appear as a result of resonant magnetic

disturbing fields, acting on the equilibrium magnetic field which contains the plasma. The ergodic limiter consists of a grid-shaped coil wound around the tokamak vessel and conducting a current that generates these disturbing fields. This claim is supported by theoretical as well as experimental evidences [6].

One popular way to think of a magnetic field line flow, even in magnetostatic equilibrium configurations, like those expected for ideal tokamak operation, is the Hamiltonian description. It was first observed by Kerst [7], and later by many authors [8–16], that magnetic field line equations could be rewritten as Hamilton equations, where the role of time is played by an ignorable (cyclic) coordinate.

Within this framework, the field line Hamiltonian is actually an invariant over the magnetic surfaces appearing in the MHD description of plasma equilibria. In dynamical systems language, they are KAM surfaces, and their existence depends on the symmetry of the equilibrium configuration [17]. The inverse winding numbers characterizing these surfaces are also known in the plasma literature as 'safety factors', since they are related to the stability of certain undesirable modes. According to this classification, magnetic surfaces are rationals (irrationals) if their safety factors are rationals (irrationals) likewise.

A magnetostatic perturbation, like that due to an ergodic limiter, can be viewed as a Hamiltonian perturbation, whose effect depends on the character of the magnetic (KAM) surface. Rational surfaces will be destroyed, leaving a chain of Poincaré–Birkhoff islands, whereas most of the irrational tori will survive, provided the hypotheses of the KAM theorem are fulfilled [18, 19]. Note that it is essential that the perturbation causes symmetry breaking in the equilibrium configuration, otherwise the island chain destruction does not occur, and the island evolution may show a completely different behaviour [20].

A useful tool to study such near-integrable systems is the Poincaré surface of section method. Magnetic (KAM) surfaces appear as invariant closed curves, and chaotic magnetic field lines yield area-filling orbits in Poincaré sections [21]. In this paper we analyse the ergodic magnetic limiter action through a couple of approaches that use Poincaré maps as preliminary diagnostics of chaos.

The first approach describes magnetic island formation by means of a linearization of field line equations in the neighbourhood of a rational surface. The method is applicable to any magnetostatic perturbation, once its Fourier components are known. The net results are a reliable estimate of magnetic island width, which is an important ingredient in any global stochasticity prescription, like the Chirikov overlapping criterion. Results are compared with Poincaré maps obtained through numerical integration of field line equations, showing a fairly good accordance. In this case, the ergodic limiter is modelled as a square-wave perturbation.

The second way to generate Poincaré maps in this context is to suppose that the ergodic limiter action on the field lines, which in the equilibrium twist freely on the magnetic surfaces, behaves as a periodic sequence of delta function pulses. This kind of procedure enables us to obtain analytical formulae for the Poincaré maps [22]. However, in its original form, this map is not exactly area-preserving, so that we have to transform the Poincaré map into a symplectic one, since it is needed to ensure flux conservation.

This paper is organized as follows: in Section 2 we describe the basic geometry to be used, and present the equilibrium as well as perturbing fields; in Section 3 the construction of Poincaré maps for field lines is carried out through the use of two methods—numerical integration of field line equations using an square-pulse waveform, and an impulsive perturbation leading to analytical expressions for the maps. The results concerning these two approaches are presented in Section 4. Section 5 is devoted to a detailed analysis of magnetic island width. Our conclusions are left to the final section.

TOKAMAK AND LIMITER MAGNETIC FIELDS

A tokamak is a toroidal vessel in which a plasma is confined by the combined action of two basic magnetic fields: the toroidal field $\mathbf{B}_T$, generated by external coils, and the poloidal field $\mathbf{B}_P$, which is produced by the plasma current itself. The equilibrium magnetic field is thus $\mathbf{B}^{(0)} = \mathbf{B}_T + \mathbf{B}_P$. One of the convenient systems of coordinates to deal with tokamak geometry is the so-called local or pseudo-toroidal coordinate system (r, θ, φ), as depicted in Fig. 1(a) [23]. In this system, the toroidal and poloidal fields are written as $\mathbf{B}_T = B_\varphi \hat{e}_\varphi$ and $\mathbf{B}_P = B_\theta \hat{e}_\theta$, respectively.

The magnetic field line equations, namely, $\mathbf{B} \times \mathrm{d}\mathbf{l} = \mathbf{0}$, are given in this system by

$$\frac{\mathrm{d}r}{B_r} = \frac{r\,\mathrm{d}\theta}{B_\theta} = \frac{R_0\,\mathrm{d}\varphi}{B_\varphi}, \tag{1}$$

where $b(R_0)$ is the minor (major) tokamak radius. The aspect ratio is defined as $A = R_0/b$, and for large aspect-ratio tokamaks ($R_0 \gg b$ or $A \gg 1$) it is possible to use a periodic cylindrical approximation ($z = R_0\varphi$, see Fig. 1(b)). The effect of toroidal curvature is thus considered as a first-order correction of the toroidal field.

The equilibrium magnetic field in the cylindrical approximation is given by $B^{(0)} = (0, B_\theta^{(0)}(r), B_z^{(0)})$, where

$$B_z^{(0)} = \frac{B_0}{1 + \dfrac{r}{R_0}\cos\theta} \equiv \frac{B_0}{1 + \epsilon\cos\theta}, \tag{2}$$

and ϵ measures the strength of the toroidal effect, B_0 being the toroidal field intensity for $\epsilon = 0$. The effect of toroidal correction is thus more intense for a large radius r [24].

For obtention of the poloidal field component it is necessary to specify the plasma

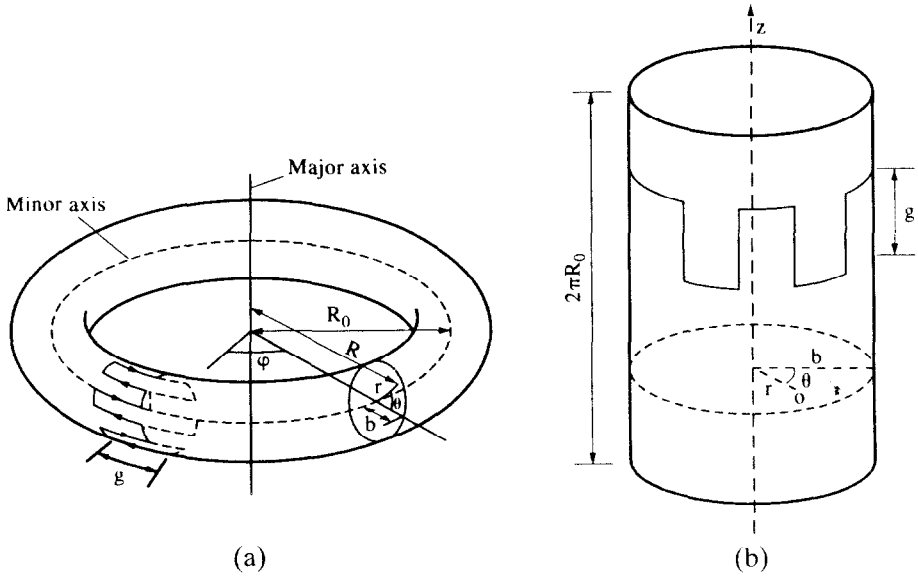

Fig. 1. Essential geometry of the tokamak and ergodic magnetic limiter.

current density profile. We will concentrate on the so-called generalized parabolic model [23] for an axisymmetric plasma current density, namely

$$\mathbf{j}_z(r) = j_0\left[1 - \left(\frac{r}{a}\right)^2\right]^\gamma \hat{e}_z, \tag{3}$$

where a is the plasma column radius (somewhat lower than minor radius); and j_0, γ are positive parameters, adjustable to fit typical tokamak discharges. Using Ampère's law, equation (3) leads to

$$B_\theta^{(0)}(r) = \frac{\mu_0 I_P}{2\pi r}\left(1 - \left[1 - \left(\frac{r}{a}\right)^2\right]^{\gamma+1}\Theta(a - r)\right), \tag{4}$$

provided I_P is the total plasmas current intensity. $\Theta(x)$ is the Heaviside unit-step function.

An important quantity related to the magnetic (KAM) surfaces is the rotational transform $\iota(r)$, defined as the average poloidal angle of displacement of a given field line in the course of a complete toroidal turn around the tokamak. Hence $\iota = 2\pi\, \mathrm{d}\theta/\mathrm{d}\varphi$, and using (1) and (4) gives for the cylindrical case ($\epsilon = 0$)

$$\iota(r) = \iota_a\left(\frac{a}{r}\right)^2\left(1 - \left[1 - \left(\frac{r}{a}\right)^2\right]^{\gamma+1}\Theta(a - r)\right), \tag{5}$$

where $\iota_a = \iota_0/(\gamma + 1)$ and ι_0 is the rotational transform at the magnetic axis ($r = 0$). In order to avoid kink instabilities, the Kruskal–Shafranov limit states that $\iota \leqslant 2\pi$ [23], so that we choose $\iota_0 = 2\pi$ and $\iota_a = (\gamma + 1)^{-1}$ for kink-stable discharges. This means that γ and I_P can be taken as independent parameters to specify plasma equilibrium.

The ergodic magnetic limiter (EML) model to be considered in this paper is the same as that already considered by Martin and Taylor [5], apart from the basic geometry which we take as cylindrical instead of rectangular. It was employed by us in previous papers [25, 26]. One EML ring consists of a grid-shaped coil of width g (see Fig. 1(a)) with $L/2$ pairs of wire pieces oriented in the (toroidal) φ-direction, and carrying a current I. Adjacent conductors have currents flowing in opposite senses, and we ignore the contributions for the magnetic field from the pieces oriented in the (poloidal) θ-direction, since their effect on the equilibrium B_z field is negligible.

Since the plasma pressure is low, we can deal only with perturbing vacuum fields, without dynamical plasma response. Ignoring border effects, the perturbing field due to such an EML device is written as $B^{(1)} = (B_r^{(1)}, B_\theta^{(1)}, 0)$, where

$$B_{r,\theta}^{(1)}(r, \theta, z) = \tilde{B}_{r,\theta}^{(1)}(r, \theta) f(z), \tag{6}$$

and $\tilde{B}_{r,\theta}^{(1)}(r, \theta)$ are evaluated supposing that the wire pieces are infinitely long, giving [26]

$$\tilde{B}_r^{(1)}(r, \theta) = \frac{-\mu_0 L I}{2\pi b}\left(\frac{r}{b}\right)^{L/2-1}\sin\left(\frac{L\theta}{2}\right) \tag{7}$$

$$\tilde{B}_\theta^{(1)}(r, \theta) = -\frac{\mu_0 L I}{2\pi b}\left(\frac{r}{b}\right)^{L/2-1}\cos\left(\frac{L\theta}{2}\right). \tag{8}$$

These results were derived from the use of a cylindrical geometry. Toroidal corrections of these fields are neglected thereby, since the EML action is very localized on the toroidal curvature.

The z-dependence of EML fields is described by the function $f(z)$, and it distinguishes

the two kinds of mappings to be discussed in this work. Firstly, we can try a square-pulse waveform:

$$f(z) = \begin{cases} 1 & \text{if } -\frac{g}{2} \leqslant z \leqslant +\frac{g}{2} \\ 0 & \text{otherwise} \end{cases} \tag{9}$$

which assumes that the limiter field falls down very sharply out of ring extension. This case will be called the *square-pulse map* (SPM).

Another possible form for $f(z)$ is a periodic sequence of delta function pulses

$$f(z) = g \sum_{j=-\infty}^{+\infty} \delta(z - 2\pi R_0 j') = \frac{g}{2\pi R_0}\left[1 + 2\sum_{k'=1}^{\infty} \cos\left(\frac{k'z}{R_0}\right)\right], \tag{10}$$

the latter form being its Fourier expansion, where the period is the tokamak length $2\pi R_0$. The map so obtained will be called the *impulsive excitation map* (IEM). Evidently, SPM and IEM cases are not mutually independent. A Fourier analysis of the square-pulse waveform (9) would render equation (10) for $g \ll R_0$ and small integer values of k'. Only within these limits is IEM suitable for description of EML action.

We also consider the case of a number $p > 1$ of EML rings, equally spaced in the toroidal direction by an angle $2\pi/p$. All EML rings are similar, the essential difference being that they have a mutual poloidal displacement, corresponding to the poloidal angle which would be completed by an equivalent helical winding. In numerical applications we restrict ourselves to the case $p = 4$. So, in the SPM case there will be four square pulses of width g centred at $z = 0$, $\pi R_0/2$, πR_0, $3\pi R_0/2$ (cf. Fig. 2(a)). In the IEM case these are the points in which a delta-kick will act on the field lines (cf. Fig. 2(b)).

OBTENTION OF POINCARÉ MAPS

Square-pulse map

Obtention of Poincaré puncture-plot maps for field lines in the square-pulse case is only feasible by numerical integration of field line equations (1), with the help of equations (4) and (7)–(9). The system of first order equations is (with $z = R_0\varphi$ as the independent variable)

$$\frac{dr}{dz} = \frac{\tilde{B}_r}{B_0} f(z)\left(1 + \frac{r}{R_0}\cos\theta\right) \tag{11}$$

$$\frac{d\theta}{dz} = \frac{1}{r}\left(\frac{B_\theta^{(0)} + \tilde{B}_\theta f(z)}{B_0}\right)\left(1 + \frac{r}{R_0}\cos\theta\right). \tag{12}$$

The Poincaré surface of the section will be located at $z = g/2$, irrespective of the number of coils p to be considered. Let (r_n, θ_n) denote the nth piercing of a given field line on this plane. We may also work with 'rectangular' coordinates defined by

$$x_n \equiv b\theta_n \qquad y_n = b - r_n, \tag{13}$$

describing the arc length at EML radius and the radial distance from the tokamak edge, respectively.

Due to magnetic flux conservation within a magnetic (KAM) surface, which stems from the Hamiltonian nature of field line equations [18], we expect that SPM would be area-preserving in the Poincaré plane; but, in fact, due to the large aspect-ratio approximation we made the system is only nearly conservative.

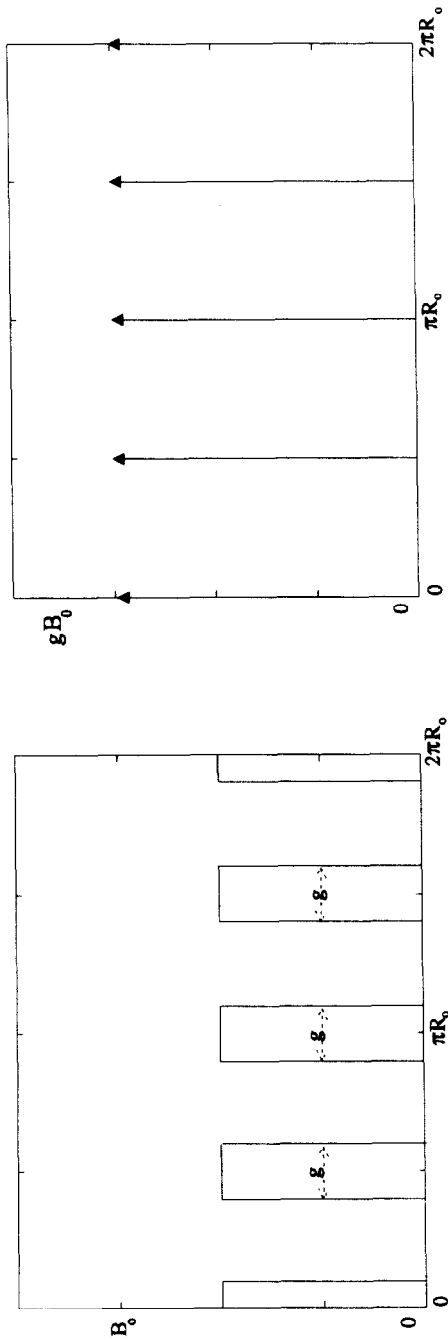

Fig. 2. z-Dependence of the radial component of EML pertubing fields.

Impulsive excitation map

The use of a periodic sequence of delta pulses enables us to obtain analytical expressions for Poincaré maps. The basic idea is that the field line twists freely, according to $\mathbf{B}^{(0)} \times \mathrm{d}\mathbf{l} = \mathbf{0}$, until it reaches the limiter at $z = 0, 2\pi R_0, \ldots 2K\pi R_0 \ldots$ (for $p = 1$ ring), or $z = 0, \pi R_0/2, \pi R_0 \ldots K'\pi R_0/2 \ldots$ (for $p = 4$ rings), when it receives a kick. This kick instantaneously changes the z-derivatives of field line coordinates (1), but not the coordinates r, θ themselves; that is, the 'velocities' $\mathrm{d}r/\mathrm{d}z$ and $\mathrm{d}\theta/\mathrm{d}z$ are discontinuous at $z = 2k'\pi$, while the coordinates are continuous [27]. The final phase portraits are taken from the Poincaré surface of the section located at $z = 0$, for any value of p, as in the previous case.

Define discretized variables for radial and angular positions of the points on the Poincaré surface of the section to be [22]

$$r_n = \lim_{\epsilon \to 0} r(z = 2\pi R_0 n + \epsilon), \tag{14}$$

$$r_n^* = \lim_{\epsilon \to 0} r(z = 2\pi R_0 (n + 1) - \epsilon), \tag{15}$$

$$\theta_n = \lim_{\epsilon \to 0} \theta(z = 2\pi R_0 n + \epsilon), \tag{16}$$

$$\theta_n^* = \lim_{\epsilon \to 0} \theta(z = 2\pi R_0 (n + 1) - \epsilon), \tag{17}$$

denoting the values of r and θ just after the nth piercing of the $z = 0$ plane, and just before the $(n + 1)$th piercing, respectively.

The part of IEM equations concerning the effect of delta kicks is [25]

$$r_{n+1} = r_n^* - \frac{\xi}{b}\left(\frac{r_n^*}{b}\right)^{m-1} \sin(m\theta_n^*), \tag{18}$$

$$\theta_{n+1} = \theta_n^* - \frac{\xi}{b^2}\left(\frac{r_n^*}{b}\right)^{m-2} \cos(m\theta_n^*), \tag{19}$$

where we have defined

$$\xi = \frac{\mu_0 m I g}{B_0 \pi}. \tag{20}$$

Since the effect of the kicks is instantaneous, between two successive kicks the field line equations are readily integrated, even in the presence of toroidal correction. In the case of the $p = 1$ limiter, we have the following expressions [25].

Cylindrical case ($\epsilon = 0$).

$$r_n^* = r_n, \tag{21}$$

$$\theta_n^* = \theta_n + \frac{2\pi B_\theta^{(0)}(r_n) R_0}{B_0}, \tag{22}$$

where the equilibrium poloidal field is given by 4. The extension of these formulae for many limiters ($p > 1$) is straightforward.

Toroidal case ($\epsilon \neq 0$).

$$r_n^* = r_n, \tag{23}$$

$$\theta_n^* = 2\arctan[\lambda(r_n)\tan(\Omega(r_n) + \arctan \Xi(r_n, \theta_n))] + 2\pi, \tag{24}$$

where we have defined the following auxiliary quantities:

$$\Omega(r_n) = \frac{\pi R_0 B_\theta^{(0)}(r_n)(1 - \epsilon(r_n))}{B_0 r_n \lambda(r_n)},$$
$$\lambda(r_n) = \frac{1 - \epsilon(r_n)}{\sqrt{1 - \epsilon^2(r_n)}}, \tag{25}$$
$$\Xi(r_n) = \frac{1}{\lambda(r_n)} \tan\left(\frac{\theta_n}{2}\right), \quad \epsilon(r_n) = \frac{r_n}{R_0}.$$

The kick mapping (18), (19) can be rewritten in terms of the following adimensional parameters

$$C = 2^{(m/2)-1} \frac{\xi}{b^2} \quad R = \frac{\frac{1}{2} r^2}{b^2}, \tag{26}$$

so that our equations for description of the field line displacement due to EML kicks are

$$(R_{n+1})^{1/2} = (R_n^*)^{1/2} - 2^{1/2} C (R_n^*)^{(m-1)/2} \sin(m\theta_n^*), \tag{27}$$

$$\theta_{n+1} = \theta_n^* - C(R_n^*)^{(m/2)-1} \cos(m\theta_n^*). \tag{28}$$

We stress that, although the mapping between two successive kicks is exact (within the limitations of our model) the part that treats a kick is obtained through a kind of approximation. Hence, this second part of the map contains higher-order terms that introduce a small dissipative effect. So, the entire IEM equations are not strictly symplectic in their original form. In order to obtain an area-preserving form for IEM, let us maintain (28) and treat (27) as a canonical transformation of variables with generating function $G(R_{n+1}, \theta_n^*)$, so that the transformation equations

$$R_n^* = \frac{\partial G}{\partial \theta_n^*}, \quad \theta_{n+1} = \frac{\partial G}{\partial R_{n+1}}, \tag{29}$$

are the necessary and sufficient conditions to be fulfilled if the mapping (27) is symplectic. Substituting (29) in (27) we find that a generating function of the form

$$G(R_{n+1}, \theta_n^*) = R_{n+1}\theta_n^* - \frac{2C}{m} R_{n+1}^{m/2} \cos(m\theta_n^*) \tag{30}$$

is suitable for this purpose. Putting (30) in (27) gives the new radial equation

$$(R_n)^{1/2} = R_{n+1} - 2C(R_n^*)^{(m-1)/2} \sin(m\theta_n^*). \tag{31}$$

This equation can be inverted for R_{n+1} only for $m = 2$ or $m = 4$ cases. In any other situation, we are forced to use the Newton method to do so, using as an initial guess for R_{n+1} the value of R_n^*. Actually the method converges very rapidly, yielding accurate results after no more than ten Newton method iterations.

PHASE PORTRAITS

In the numerical applications to be considered in this paper we take parameters from a small tokamak—the TBR-1, operating at the Physics Institiute of the University of São Paulo, Brazil. The main parameters are: $R_0 = 0.30m$ (major radius); $b = 0.11m$ (minor radius); $a = 0.08m$ (plasma radius); $B_0 = 0.50T$ (toroidal field at magnetic axis); $\iota_a = 2\pi/5$ (rotational transform at plasma edge); $\iota_0 = 2\pi$ (rotational transform at plasma centre) [28].

Let us concentrate on the case of one EML ring with $m = L/2 = 6$ pairs of wires; and suppose a ring length of $g = 0.08m$. The choice of L is motivated by the fact that a perturbation with such a value of $m = L/2$ will excite magnetic island formation in the location of magnetic surfaces characterized by rotational transforms $\iota = 2\pi n/m$, where $n = 1, 2, \ldots, m$, a result which follows from the Poincaré–Birkhoff theorem. But we want to create these islands primarily in the peripheral region of the tokamak, which comprises the outer portion of the plasma column plus the vacuum region near the inner wall. Moreover since the field created by an EML ring decreases rapidly with the distance from the inner wall, those islands with high values of n are not of interest because they are in the plasma core.

Hence, we need to know the radial profile of the rotational transform in order to specify a judicious choice of L required in the design of an EML experiment. Figure 3(a) is such a profile, obtained with the help of the TBR-1 parameters. It indicates that a convenient region to explore contains the rotational transforms $2\pi(1/6)$ and $2\pi(2/6)$, so that an EML ring with $L/2 = 6$ would excite primarily those islands.

This assumption is well supported by phase portraits obtained with the use of both SPM and IEM formulae. All parameters are taken from TBR-1. Figure 4 shows the case of the $p = 1$ limiter, carrying a current of $I = 400$ A and without toroidal correction ($\epsilon = 0$). The SPM (Fig. 4(a)) and IEM (Fig. 4(b)) phase portraits are very similar. Note that IEM orbits are more well-defined than SMP due to the large number of iterations allowed by analytical mappings, in contrast with a map generated by numerical integration of field line equations. Nevertheless, two primary magnetic island chains are clearly observed—the 6/1 chain, located roughly around the surface at $y_0 = 0.025m$ (where $y_0 = b - r_0$); and the 6/2 chain, located near the radial position of $y_0 = 0.050m$. There is a little difference between SPM and IEM with respect to the numerical values for this location. Moreover, in both models the 6/2 resonances are substantially shorter than the 6/1 resonances. The reason for this fact is the abrupt decrease of the perturbing field with the distance from the inner wall. Hence, although more resonances are expected to appear, only these ones are relvant in the analysis of EML performance.

Figure 5 shows phase portraits for the $p = 1$ ring and $I = 400$ A, but with toroidal correction (2), i.e., ($\epsilon \neq 0$). Both maps, SPM (Fig. 5(a)) and IEM (Fig. 5(b)) show a richer variety of islands, in contrast with the previous case, where the pure cylindrical case was considered. Previous analysis of Poincaré maps for field lines with perturbations of a helical winding type [20, 29] shows the presence of 'satellite' or secondary island chains in the vicinity of the primary resonances; a fact already expected from theoretical arguments [30, 31]. Apart from differences caused by graphical definition, both maps exibit satellite chains of $m = 6$, $m = 7$ and even $m = 8$ in the vicinity of 6/1 and 6/2 primary resonances of the preceeding case.

The multiplicity of higher-order resonances leads to various overlappings between adjacent islands and field-line stochasticity. The chaotic nature of some orbits, whose initial conditions belong to stochastic layers, can be inferred from the power spectrum of the field line trajectories on the Poincaré plane. Figure 6 shows such power spectra for an orbit generated by the point $x_0 = 0.34560m$, $y_0 = 0.03130m$, for SPM (Fig. 6(a)) and IEM (Fig. 6(b)). The presence of a broadband noise spectra highly concentrated at low frequencies indicates chaos.

The case of $p = 4$ limiter rings and no toroidal effect (cf. Fig. 7(a)) for SPM and Fig. 7(b)) for IEM) leads to phase portraits qualitatively similar to those shown in Fig. 4 (for $p = 1$), but with larger resonances, for the same value of EML current ($I = 400$ A). This result stems from the theoretical formula to be derived in the next section, for the width of a primary magnetic island generated by EML field. Figure 8 exhibits the same

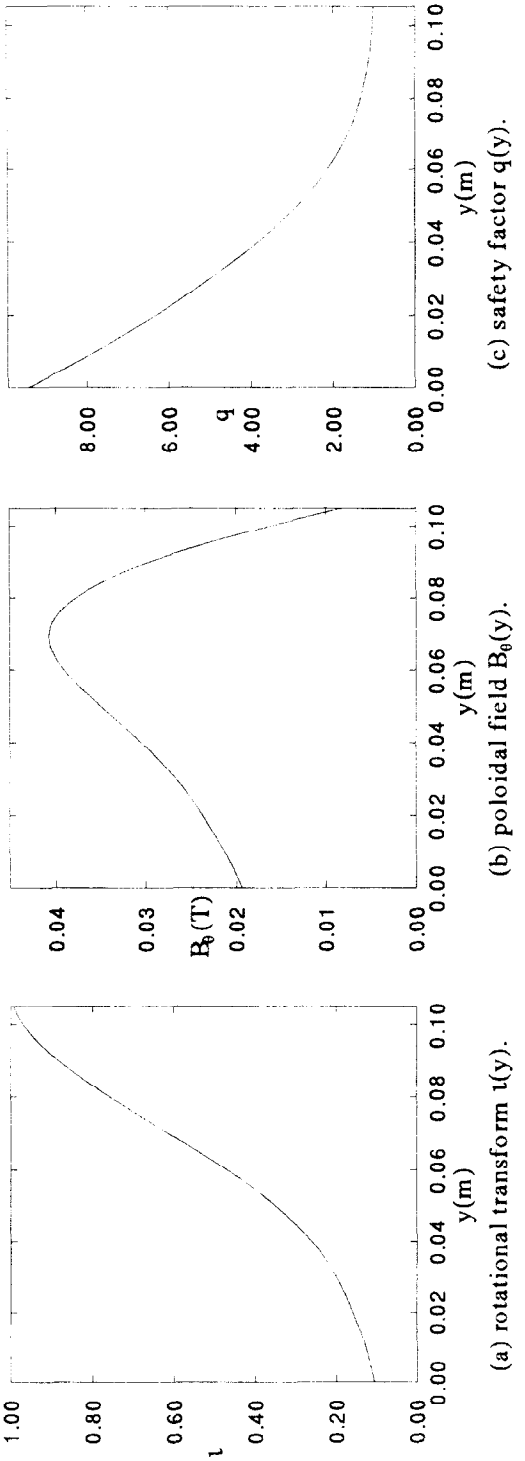

Fig. 3. Radial profiles of plasma equilibrium in a large aspect ratio tokamak with TBR-1 parameters.

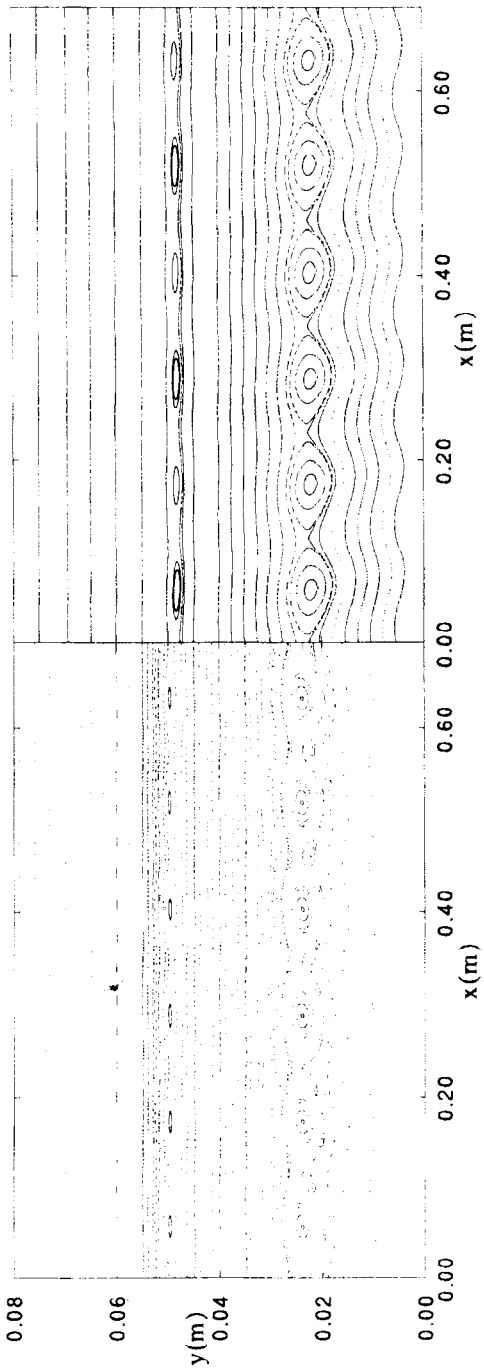

Fig. 4. Phase portraits for the $p = 1$ EML ring with $I = 400$ A, without toroidal correction ($\varepsilon = 0$), and TBR-1 parameters.

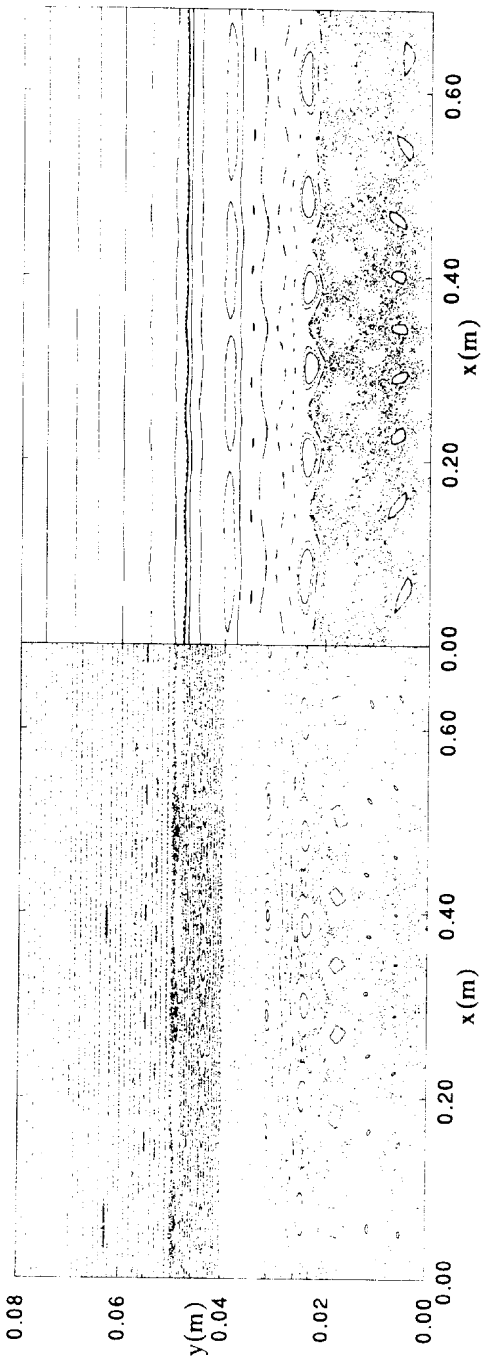

Fig. 5. Phase portraits for the $p = 1$ EML ring with $I = 400$ A, without toroidal correction ($\varepsilon > 0$), and TBR-1 parameters.

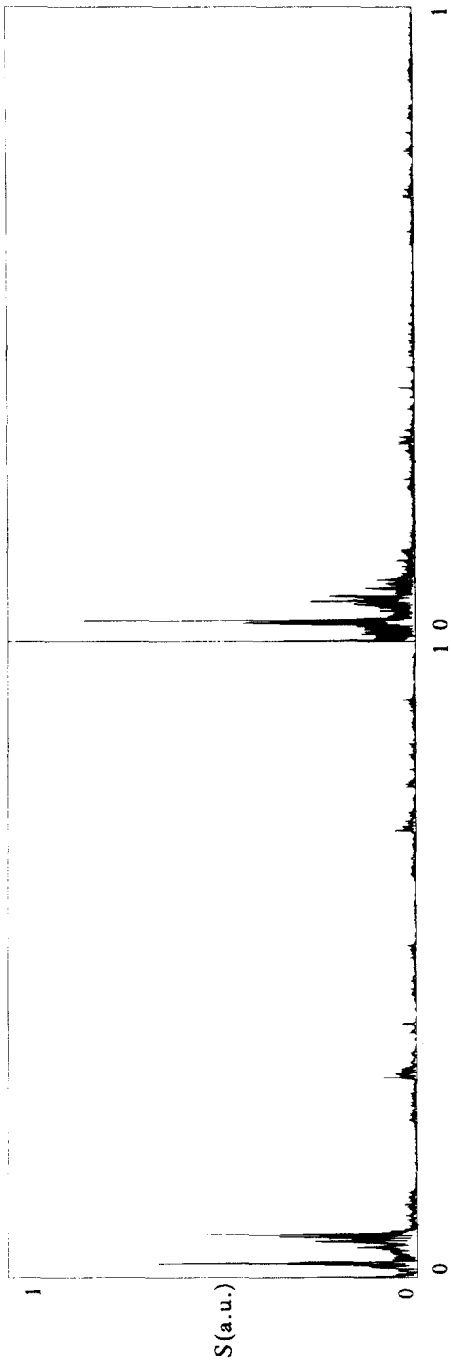

Fig. 6. Power spectra of the trajectories for the case depicted in Fig. 5 with $x_0 = 0.3456m$ and $y_0 = 0.0313m$.

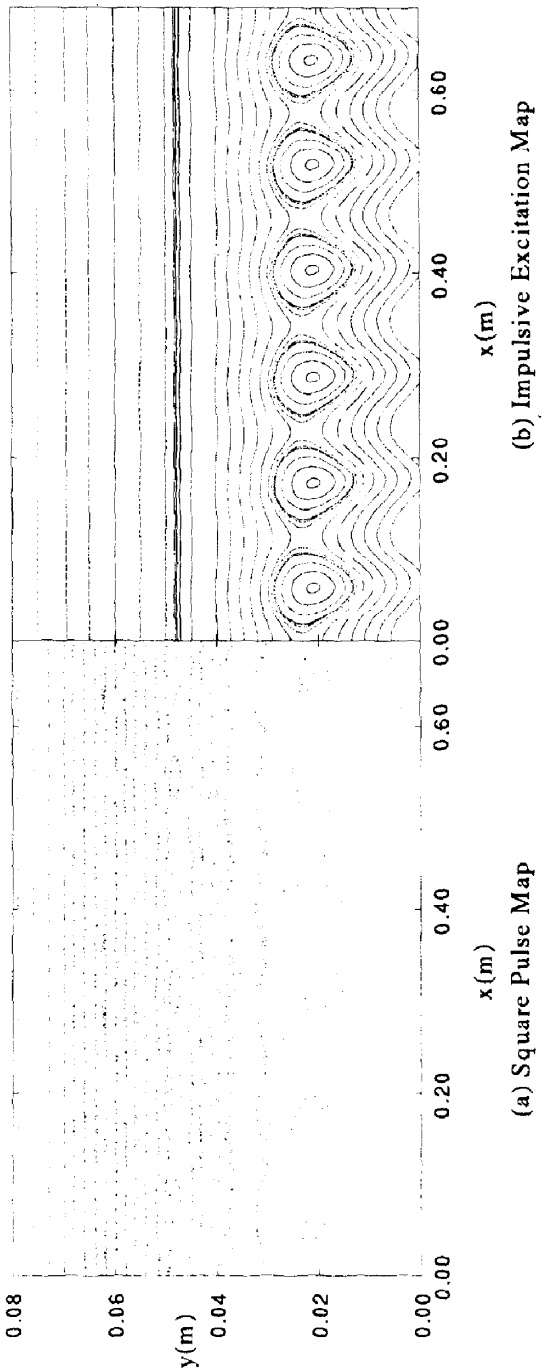

Fig. 7. Phase portraits for $p = 4$ EML rings with $I = 400$ A, without toroidal correction ($\varepsilon = 0$), and TBR-1 parameters.

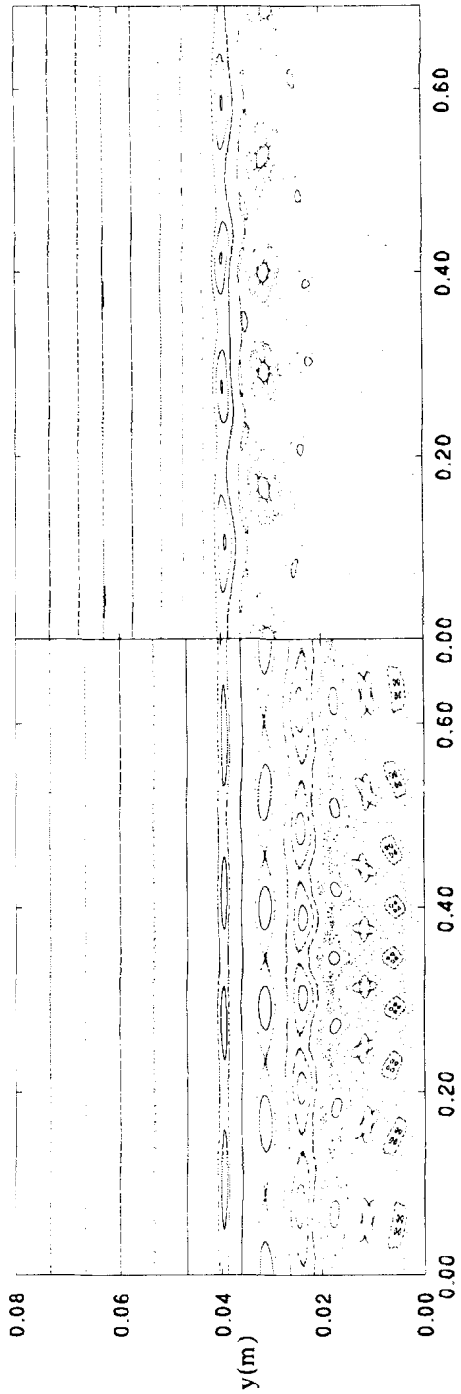

Fig. 8. Phase portraits for $p = 4$ EML rings with toroidal correction ($\varepsilon > 0$), and TBR-1 parameters.

case, but now with toroidal correction ($\epsilon \neq 0$), which presents an enlarged stochasticity region in the peripheral region of the tokamak, according to the expected performance for EML. Only the IEM case is presented, since the numerical integration required for obtention of the SPM phase portrait is not convenient for magnification of finer details in the stochastic regions, when the perturbation strength is too high. This would be achieved introducing a symplectic integration procedure.

MAGNETIC ISLAND WIDTHS

The width of a magnetic island obtained in the SPM case can be estimated by the theoretical method developed by Matsuda and Yoshikawa to deal with general error fields [32]. We assume a cylindrical geometry ($\epsilon = 0$), but allow the existence of an arbitrary number p of EML rings. Let r_0 be the radial position of a given resonant magnetic surface. A set of islands will appear around this point, after a suitably chosen perturbation is switched on. Linearizing $\iota(r)$ in the neighbourhood of this surface gives

$$\frac{d\theta}{d\varphi} \approx \frac{1}{2\pi}(\iota_0 + \iota' x), \tag{32}$$

where $x = r - r_0$, $\iota_0 = \iota(r_0)$ and $\iota' = (d\iota/dr)_{r=r_0}$. If the sought-for islands are small enough, we can neglect the radial variation of perturbing fields, and evaluate them at $r = r_0$, such that (1) is written as

$$\frac{dx}{d\theta} \approx \frac{rB_r^{(1)}(r_0, \theta, \varphi)}{B_\theta^{(0)}(r_0)}. \tag{33}$$

If the radial component of the perturbing field is periodic in θ and φ, we can Fourier-expand it, as

$$B_r^{(1)}(r_0, \theta, \varphi) = \sum_{m,n} \mathcal{B}_{mn} e^{i(m\theta - n\varphi)}, \tag{34}$$

but the relevant terms of this series are those which characterize resonances, so as to satisfy the relation $\iota_0 = 2\pi n/m$, where m and n are co-prime positive integers. The remaining terms oscillate very fast and vanish when averaged over typical periods of motion. Taking only one mode m/n of the perturbing field, namely

$$B_r^{(1)}(r_0, \theta, \varphi) = b_{m,n}(r_0) \sin(m\theta - n\varphi + \beta), \tag{35}$$

where $b_{m,n}$ and β are related to the Fourier coefficients of (35), equation (32) gives in the neighbourhood of the resonance at $r = r_0$

$$\frac{d\alpha}{d\varphi} = m - \frac{2\pi n}{\iota_0 + \iota' x}, \tag{36}$$

where $\alpha = m\theta - n\varphi + \beta$. Combining (36) with (33), when $\iota' x/\iota_0 \ll 1$ one finds

$$\frac{d^2\alpha}{d\theta^2} = -A \sin \alpha, \tag{37}$$

where we have defined

$$A = -\frac{2\pi n \iota' r_0 b_{m,n}(r_0)}{\iota_0^2 B_\theta^{(0)}(r_0)}. \tag{38}$$

One recognizes (37) as the equation of a nonlinear pendulum, which is a paradigm for the motion around any type of resonance, as is shown in canonical perturbation theory [18]. The advantage here is that (37) is obtained directly from the field line equations (1). A different approach would be the use of Hamiltonian perturbation theory for field lines, which gives essentially the same results [26]. The qualitative aspects of the solution curves of (37) are well known. Working with the adimensional parameter $k^2 = E/2A$, where $E = (1/2)(\mathrm{d}\alpha/\mathrm{d}\theta)^2_{\alpha=0}$, we have three distinct types of solutions, according to its value: rotation curves ($k^2 > 1$), liberation curves ($k^2 < 1$) and a separatrix ($k^2 = 1$), which bounds a magnetic island (in the Poincaré plane $\varphi = 0$).

Furthermore, one can evaluate the island width $\delta_{m/n}$ (in tokamak coordinates) by integration of equation (33) over a complete turn of the phase α. Using (37) we obtain [32]

$$\delta_{m/n} = \int_{\text{island}} \frac{\mathrm{d}x}{\mathrm{d}\theta}\,\mathrm{d}\theta = 4r_0\left(\frac{b_{mn}}{mB_\theta^{(0)}(r_0)}\left|\frac{\iota_0}{-r_0\iota'}\right|\right)^{1/2}. \tag{39}$$

In order to apply the above equation, it is necessary to know the appropriate Fourier coefficient of the radial error field from its double trigonometric series

$$\begin{aligned} B_r^{(1)} = \sum_{m',n'} \Bigg\{ & A_{m',n'} \cos\left(\frac{2\pi m'\theta}{T_1}\right)\cos\left(\frac{2\pi n'\varphi}{T_2}\right) \\ & + B_{m',n'} \sin\left(\frac{2\pi m'\theta}{T_1}\right)\sin\left(\frac{2\pi n'\varphi}{T_2}\right) + D_{m',n'} \cos\left(\frac{2\pi m'\theta}{T_1}\right)\sin\left(\frac{2\pi n'\varphi}{T_2}\right) \\ & + E_{m',n'} \sin\left(\frac{2\pi m'\theta}{T_1}\right)\cos\left(\frac{2\pi n'\varphi}{T_2}\right)\Bigg\}, \end{aligned} \tag{40}$$

where T_1 and T_2 are the fundamental periods of variation for angle variables θ and φ, respectively. This form of Fourier expansion is related to the original series (34) by the following definitions:

$$m = \frac{2\pi m'}{T_1} \qquad n = \frac{2\pi n'}{T_2}. \tag{41}$$

If the rings are assembled with an angular displacement of $2\pi/p$ around the torus, $B_r^{(1)}$ is symmetric by the change $\varphi \to -\varphi$, so that there is only one non-vanishing Fourier coefficient in (40),

$$E_{m',n'} = \frac{4}{T_1 T_2}\int \mathrm{d}\theta \int \mathrm{d}\varphi B_r^{(1)}(r_0, \theta, \varphi)\sin\left(\frac{2\pi m'\theta}{T_1}\right)\cos\left(\frac{2\pi n'\varphi}{T_2}\right). \tag{42}$$

Taking into account the z-dependence characteristic of the square-pulse map (cf. Fig. 3(a)), a simple integration gives

$$E_{m',n'} = \frac{4p}{2\pi^2}\Lambda(r_0)\pi\delta_{L/2,m'}\left(\frac{2}{pn'}\right)\sin\left(\frac{pn'g}{2R_0}\right), \tag{43}$$

where

$$\Lambda(r_0) = \frac{\mu_0 IL}{2\pi b}\left(\frac{r_0}{b}\right)^{L/2-1}. \tag{44}$$

Now working with the safety factor $q(r) = 2\pi/\iota(r)$, in the resonant surface we get $m = q(r_0)n$, with $m = m'$ and $n = pn'$. The resonance conditions turn out to be

$$n' = \frac{n}{p} \qquad m' = m = qn = \frac{L}{2}. \tag{45}$$

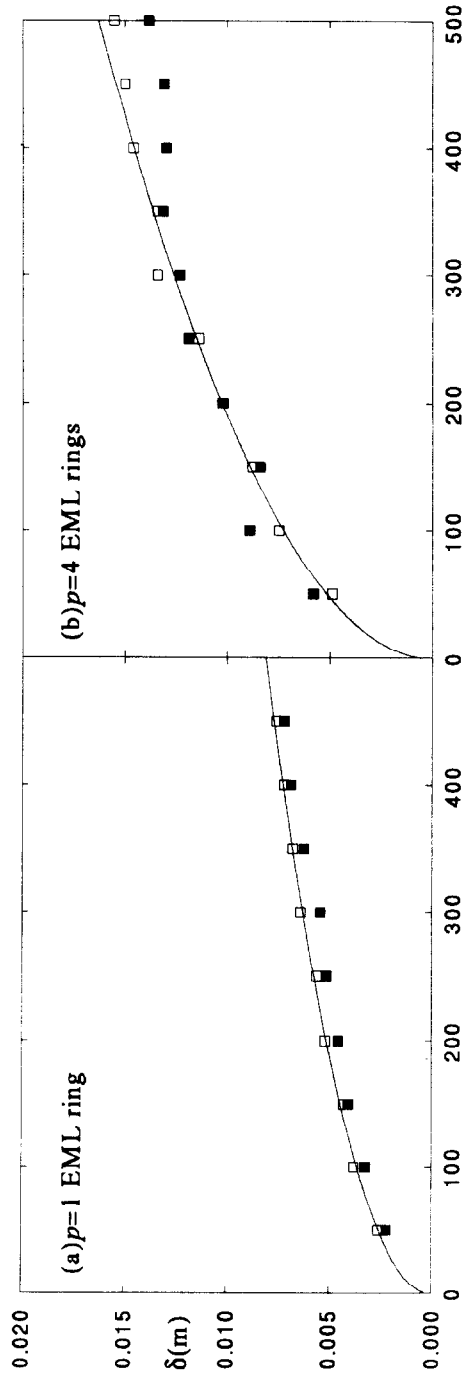

Fig. 9. Magnetic island width for 6/1 resonance, calculated using equation (39) with TBR-1 parameters. Full boxes represent SPM and empty boxes IEM.

in such a way that the mode coefficient necessary for island width evaluation reads

$$b_{m,n}(r_0) = \frac{p}{\pi n}\left(\frac{\mu_0 IL}{2\pi b}\right)\left(\frac{r_0}{b}\right)^{qn-1} \sin\left(\frac{ng}{2R_0}\right). \tag{46}$$

Figure 9 shows a comparison between the theoretical prediction that we have been made with help of (39), for SQM constructed with $p = 1$ and $p = 4$ limiter rings. Parameters are taken from TBR-1, with the equilibrium model studied in Section 2. Island widths measured directly from phase portraits are indicated as boxes in the figure. The resonance width increases with the square root of the EML current as well as with the number of rings, and varies inversely with the magnetic shear. For instance, islands obtained with $p = 4$ limiters are twice as large as those obtained with only a $p = 1$ ring, for the same value of current intensity.

The agreement between our theoretical model and Poincaré maps of the SPM type is quite good, within the limitations inherent to the various approximate models involved. The small deviations can be partially explained by width measurements without taking account of the stochastic separatrix layer, because the separatrix itself is not well-defined in the presence of perturbations.

CONCLUSIONS

Poincaré maps for magnetic field lines have been a useful theoretical tool for plasma physicists, since they reveal the basic dynamical phenomena without detailed description of the whole three-dimensional MHD problem. The most frequent method to generate these maps has been the numerical integration of field line equations, which is a time consuming task, and with cumulative numerical errors that introduce small deviations to the symplectic nature of the maps. Analytical expressions are thus of great interest, from the theoretical point of view.

The ergodic magnetic limiter problem has been an important laboratory to study dynamical properties of maps, since it is designed to generate bounded chaotic field line layers. In this work we approach this problem from two ways, making comparisons between maps which have been obtained through numerical integration as well as analytical formulae. The basic difference between these cases is the form of toroidal dependence of the limiter perturbing field. Assuming a delta function shaped perturbation enables us to write explicit formulae for the map, which becomes rigorously symplectic after a canonical transformation is applied.

Results are in good agreement with numerical maps which use square-pulse perturbations, provided the approximations we made remain valid in both cases. The main prediction of the ergodic limiter model, namely, the onset of a chaotic region of field lines, appears in the analysis of power spectra. Moreover, the magnetic island width and radial location of primary resonances generated by perturbation is estimated, results being in accordance with phase portraits of the square-pulse map.

These results can be a basis for further investigations of field line diffusion in the peripheral region of the tokamak, in order to elucidate particle and heat transport properties in the plasma edge, where a very turbulent phase has been detected by many experiments.

Acknowledgements—I. L. C. and R. L. V. were partially supported by CNPq and FAPESP (Brazilian Government Agencies). J. M. P. was supported by CAPES and K. U. was supported by FAPESP. The authors would like to thank Dr C. Ferro-Fontan (Facultad de Ciencias Exactas e Naturales, Universidad de Buenos Aires) for useful discussions.

REFERENCES

1. A. J. Wootton, B. A. Carreras, H. Matsumoto, K. McGuire, W. A. Peebles, Ch. Ritz, P. W. Terry and S. J. Zweben, Fluctuations and anomalous transport in tokamaks, *Physics of Fluids B* **2**, 2879 (1990).
2. F. Wagner and U. Stroh, Transport in toroidal devices—the experimentalist's view, *Plasma Physics and Controlled Fusion* **35**, 1321 (1993)
3. W. Feneberg, The use of external helical winding for the production of a screening layer in ASDEX and a tokamak with material limiter, in *Proceedings of 8th European Conference of Controlled Fusion and Plasma Physics (Praha, 1977)*, Vol. **1**, p. 3 (1977)
4. F. Karger and K. Lackner, Resonant helical divertor, *Physics Letters A* **61**, 385 (1977).
5. T. J. Martin and J. B. Taylor, Ergodic behaviour in a magnetic limiter, *Plasma Physics and Controlled Fusion* **26**, 321 (1984).
6. S. McCool *et al.*, Electron thermal confinement studies with applied resonant fields on TEXT, *Nuclear Fusion* **29**, 547 (1989).
7. D. W. Kerst, The influence of errors on plasma-confining magnetic fields, *J. Nuclear Energy, Part C* **4** 253 (1962)
8. K. J. Whiteman, Invariants and stability in classical mechanics, *Reports of Progress in Physics* **40**, 1033 (1977).
9. N. N. Filonenko, R. Z. Sagdeev and G. M. Zaslawsky, Destruction of magnetic surfaces by magnetic field irregularities: Part II, *Nuclear Fusion* **7**, 253–266 (1967).
10. R. P. Freis, C. W. Hartman, F. M. Hamzeh and A. J. Lichtenberg, Magnetic island formation and destruction in a levitron, *Nuclear Fusion* **13**, 533 (1973).
11. K. Elsaesser, Magnetic field line flow as a Hamiltonian problem, *Plasma Physics and Controlled Fusion* **28**, 1743 (1986).
12. J. T. Cary and R. G. Littlejohn, Noncanonical Hamiltonian mechanics and its application to magnetic field line flow, *Annals of Physics* **151**, 1–34 (1983).
13. R. L. Viana, Comments on the Hamiltonian representation for helically symmetric magnetic fields, *Plasma Physics and Controlled Fusion* **36**, 587 (1994).
14. R. L. Viana, Hamiltonian representation for magnetic field lines in an exactly soluble model, submitted to the *Brazilian Journal of Physics*.
15. R. L. Viana and I. L. Caldas, Comment on the magnetic field generated by an infinite current grid, *European J. Physics* **12** 293 (1991).
16. R. L. Viana, Magnetic field line Hamiltonians for some perturbed MHD equilibria in cylindrical coordinates, *Revista Mexicana de Física* **39**, 902 (1993).
17. J. M. Greene and J. L. Johnson, Hydromagnetic equilibrium and stability, in *Advances in Theoretical Physics*, edited by K. A. Brueckner, Vol. 1. Academic Press, New York (1965).
18. A. L. Lichtemberg and M. A. Lieberman, *Regular and Stochastic Motion*. Springer, New York (1983).
19. M. D. Kruskal and R. M. Kulsrud, Equilibrium of a magnetically confined plasma in a toroid, *Physics of Fluids* **1**, 265–274 (1958).
20. G. A. Oda and I. L. Caldas, Dimerized island chains in tokamaks, *Chaos, Solitions & Fractals* **5**, 15 (1995).
21. A. J. Lichtemberg, Stochasticity as the mechanism for the disruptive phase of the $m = 1$ tokamak oscillations, *Nuclear Fusion* **24**, 1277 (1984).
22. I. L. Caldas and H. Tasso, Limit cycles of periodically forced oscillations, *Physics Letters A* **135**, 264–266 (1989).
23. J. P. Friedberg, *Ideal Magnetohydrodynamics*. Plenum Press, New York (1987).
24. H. D. Hazeltine and J. D. Meiss, *Plasma Confinement*. Addison–Wesley, New York (1992).
25. R. L. Viana and I. L. Caldas, Peripheral stochasticity in tokamaks—the Martin–Taylor model revisited, *Zeitschrift für Naturforschung* **47**, 941 (1992).
26. R. L. Viana and J. M. Pereira, Hamiltonian approach for magnetic surfaces in a tokamak with non-symmetric perturbations, submitted to *Rev. Mex. Física*.
27. F. J. Romeiras, C. Grebogi, E. Ott and W. P. Dayawansa, Controlling chaotic dynamical systems, *Physica D* **58**, 165 (1992).
28. I. C. Nascimento, I. L. Caldas and R. M. O. Galvão, Tokamak research at University of São Paulo, *J. Fusion Energy* **12**, 529 (1994).
29. A. S. Fernandes, M. V. A. P. Heller and I. L. Caldas, The destruction of magnetic surfaces by resonant helical fields, *Plasma Physics and Controlled Fusion* **30**, 1203 (1988).
30. B. V. Chirikov, A universal instability of many-dimensional oscillator system, *Physics Reports* **52**, 265–379 (1979).
31. J. M. Finn, The destruction of magnetic surfaces in tokamaks by current perturbations, *Nuclear Fusion* **15**, 845 (1975).
32. S. Matsuda and M. Yoshikawa, Magnetic island formation due to error field in the JFT-2 tokamak, *Japanese J. Applied Physics* **14**, 87 (1975).